ORIGINAL ARTICLE

lajss.org© Latin American Journal of Solids and Structures

www.lajss.org

Element Strain Energy Density Factor Approach to Assess Fracture and Fatigue Crack Growth

Zhao Fang[a,b], Fan Yang[c], Sheng Shen[c], Aiqun Li[c,d]*, Jingwen Yu[a]

[a] School of Civil Engineering and Architecture, Nanjing Institute of Technology, Nanjing 211167, China. Email: phoenix.fang@hotmail.com, 2100727629@qq.com

[b] Jiangsu University Key Laboratory of Intelligent Construction and Smart Operation & Maintenance of Power Infrastructure (Nanjing Institute of Technology), Nanjing 211167, China.

[c] School of Civil Engineering, Southeast University, Nanjing 210096, China. Email: 230169381@seu.edu.cn, ss13seu@gmail.com, liaiqun@bucea.edu.cn

[d] Beijing Advanced Innovation Center for Future Urban Design, Beijing University of Civil Engineering and Architecture, Beijing 100044, China.

* Corresponding author

https://doi.org/10.1590/1679-7825/e9073

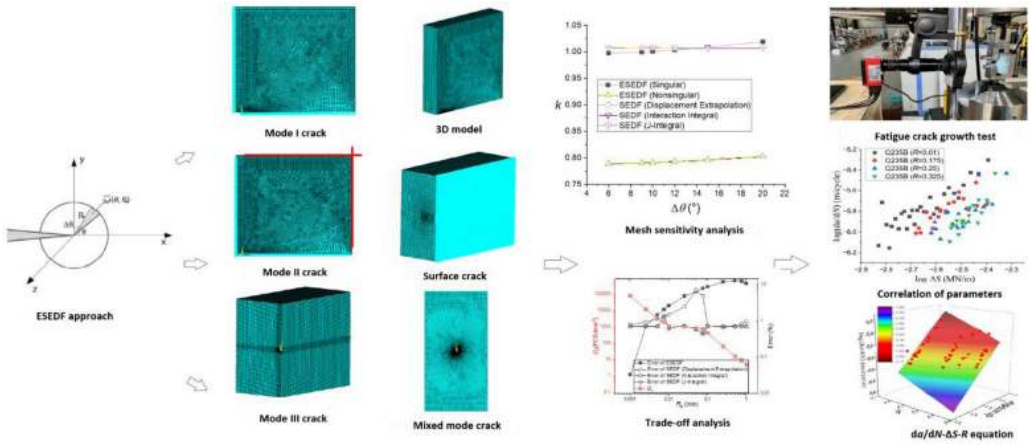
Abstract

A new finite element (FE)-based approach for calculating crack-tip strain energy density factor (SEDF) named "element strain energy density factor (ESEDF) approach" was proposed. Mode I, mode II, mode III and mixed mode cracks in both 2D models and 3D models were analyzed. A da/dN-ΔS-R equation considering stress ratios was proposed for mode I cracks and a fatigue crack growth test was done. The results show that the ESEDF approach directly computes SEDF from FE results without assuming plane stress/strain or calculating stress intensity factors. It performs best for regular mode I/II cracks in 2D and 3D models, but is less accurate for complex mixed-mode, 3D mode III, surface-cracks and coarse-mesh cases, while remaining acceptable accuracy. The proposed da/dN-ΔS-R equation correlates fatigue crack growth rate with SEDF ranges considering stress ratios in mode I cracks for steels well.

Keywords

element strain energy density factor approach; strain energy density factor; linear elastic fracture mechanics; stress intensity factor

Graphical Abstract



Received April 13, 2026. In revised form May 06, 2026. Accepted June 22, 2026. Available online June 25, 2026.
https://doi.org/10.1590/1679-7825/e9073

Latin American Journal of Solids and Structures. ISSN 1679-7825. Copyright © 2026. This is an Open Access article distributed under the terms of the Creative Commons Attribution License, which permits unrestricted use, distribution, and reproduction in any medium, provided the original work is properly cited.

1 INTRODUCTION

Fatigue failure has been widely reported in engineering industries and contributes to structural damage. The fatigue crack growth describes the period from the appearance of visible fatigue cracks to the final fracture, analyzed mainly based on linear elastic fracture mechanics. The conventional crack growth rate assessment is based on the combination use of stress intensity factor (SIF) and Paris law (known as *K* criterion), which is a rather mature method adopted in series of codes and standards, including ASTM E647 (1995), GB/T 6398-2017 (2017), IIW-2259-15 (2016), DNVGL-RP-C203 (2016).

Alternatively, to conduct fatigue crack growth life assessment using strain energy density (SED) is another alternative and has received more attention in recent decades. Sih (1974) and Sih and Macdonald (1974) proposed the strain energy density factor (SEDF) criterion (known as *S* criterion). They pointed out that the use of the SEDF *S* in the location at a specific critical distance away from the point of singularity at the crack tip was a promising way to solve linear elastic fracture mechanics problem, as shown in Equation (1):

$$S = \omega \cdot r = a_{11}K_{\mathrm{I}}^2 + 2a_{12}K_{\mathrm{I}}K_{\mathrm{II}} + a_{22}K_{\mathrm{II}}^2 + a_{33}K_{\mathrm{III}}^2 \tag{1}$$

where ω is the SED of the location at a distance of *r* away from the crack tip; K_{I}, K_{II} and K_{III} are the SIF under mode I, mode II and mode III crack loading conditions. The parameters of a_{11}, a_{12}, a_{22} and a_{33} are coefficients calculated by Equations(2)-(5), where the shear modulus *G* and the coefficient κ are calculated by Equation (6) and Equation (7) depending on the elastic modulus *E* and Poisson's ratio v; ϑ is the polar coordinate as shown in Figure1(a).

$$a_{11} = \frac{1}{16\pi G}(1 + cos\theta)(\kappa - cos\theta) \tag{2}$$

$$a_{12} = \frac{1}{16\pi G} sin\theta[2cos\theta - (\kappa - 1)] \tag{3}$$

$$a_{22} = \frac{1}{16\pi G}[(\kappa + 1)(1 - cos\theta) + (1 + cos\theta)(3cos\theta - 1)] \tag{4}$$

$$a_{33} = \frac{1}{4\pi G} \tag{5}$$

$$G = E/2(1 + v) \tag{6}$$

$$\kappa = \begin{cases} 3 - 4v, \text{plane strain state} \\ (3 - v)/(1 + v), \text{plane stress state} \end{cases} \tag{7}$$

Later, Sih (1984) extended his theory into fatigue crack growth rate analysis using the SEDF range ΔS as shown in Equation (8):

$$\frac{da}{dN} = C(\Delta S)^n \tag{8}$$

$$\Delta S = S_{max} - S_{min} \tag{9}$$

where *n* and *C* are both material-related coefficients; *a* is the crack length and *N* is the cycle number.The effect of the stress ratio *R* is considered using the mean value of SIFs, by substituting Equation (1) into Equation (9), as shown in Equation (10):

$$\Delta S = 2[a_{11}\overline{K_{\mathrm{I}}}\Delta K_{\mathrm{I}} + a_{12}(\overline{K_{\mathrm{II}}}\Delta K_{\mathrm{I}} + \overline{K_{\mathrm{I}}}\Delta K_{\mathrm{II}}) + a_{22}\overline{K_{\mathrm{II}}}\Delta K_{\mathrm{II}} + a_{33}\overline{K_{\mathrm{III}}}\Delta K_{\mathrm{III}}] \tag{10}$$

where $\overline{K_{\mathrm{I}}}$, $\overline{K_{\mathrm{II}}}$ and $\overline{K_{\mathrm{III}}}$ are the mean value of SIFs under each crack mode; ΔK_{I}, ΔK_{II} and ΔK_{III} are the range of SIFs under each crack mode.

Badaliance (1980) proposed a more comprehensive equation correlating fatigue crack growth rate da/dN with SEDF range ΔS considering the effect of the stress ratio R as shown in Equation (11),

$$\frac{da}{dN} = \exp\left\{C_1 \frac{[A\ln(\alpha\Delta S) - B]}{|A\ln(\alpha\Delta S) - B|} |A\ln(\alpha\Delta S) - B|^n + C_2[A\ln(\alpha\Delta S) - B]^2 + C_3|A\ln(\alpha\Delta S) - B| + C_4\right\} \tag{11}$$

where α is an empirical parameter devised to account for the effect of stress ratio and it is as shown in Equation (12):

$$\alpha = (1 + R)\Big/\left\{1 + R\left[\frac{\sigma_{\mathrm{u}}(1+\%RA)}{\sigma_{\mathrm{y}}}\right]^2\right\} \tag{12}$$

where $\%RA$ is the percentage reduction in area; σ_{u} is the ultimate stress; σ_{y} is the yield stress of a standard tensile specimen; A, B, C_1, C_2, C_3, C_4 and n are material-dependent constants.

The proposal of SEDF criterion was notable work and the following researchers continued to further extend this criterion. Some of the researchers adjusted this criterion from theoretical views to consider more affecting factors. Ayatollahi and Sedighiani (2012) studied the minimum SEDF criterion with the consideration of the effect of T-stress on the critical mode I SIF of brittle and quasi-brittle materials; Wei (2012) extended the criterion for crack kinks and material failure by weighting differently the volumetric and distortional parts in the extended SEDF; Boulenouar et al. (2013) conducted FE simulation of crack growth under mixed mode loading by displacement extrapolation method and SEDF theory; Shlyannikov et al. (2015) simulated a mode I fracture of single-edge-notched bend and compact specimens by total SED with the consideration of both elastic and plastic parts and studied the critical distance behavior; Ayatollahi et al. (2015) proposed a modified mixed mode fracture model to predicate the fracture resistance in brittle and quasi-brittle materials. Inspired by the idea of SEDF, the averaged SED criterion was proposed by Lazzarin and Zambard (2001) and it was proved to be powerful for assessing the strength of notched and welded structures under static and fatigue loading conditions by Berto and Lazzarin (2014), Berto et al. (2016) and Razavi et al (2018).

In addition to the innovation in SEDF criterion, the following researchers applied this criterion to various materials and engineering components. Zhou (2006) used the criterion in conjunction with a micromechanics model to investigate the condition and direction of shear failure for brittle rock subjected to triaxial compression; Hamdi et al. (2007) dealt with the fracture of rubbers under a mixed mode loading; Fang et al. (2007) investigated the multiple scattering of shear waves and SED in a semi-infinite slab of functionally graded materials with a circular cavity; Fajdiga et al. (2007) analyzed the surface initiated crack growth in the lubricated contact area of meshing gears by the criterion. Ayatollahi et al. (2011) used it to study the effects of multi-walled carbon nanotubes on fracture behavior of epoxy under mixed mode loading; Li et al. (2013) introduced a simple method for calculating SIFs of transverse cracked shaft subjected to tension, bending and shear; Feng et al. (2014) investigated a central crack problem for a functionally graded superconducting film with the applied transport currents; Cao et al. (2016) analyzed the fracture property of 7050 aluminum alloy; Aliha (2019) predicted the mode II fracture toughness of semi-circular bend specimens made of different asphalt mixtures using the SEDF criterion and compared it to test results; Khaji et al. (2022) proposed a mixed-mode I/II fracture criterion for predicting the fracture of composite materials.

Although the above literatures demonstrate that great progress has been made regarding SEDF, there are still some issues need to clarify. The first issue is that all the above literatures obtain the SEDF values from the SIF at the crack tip by Equation (1) and thus the SIF is indispensable as a medium to calculate the SEDF. It means that the SEDF criterion is still a SIF-based criterion. The first issue further brings about the second one that a plane stress state or a plane strain state has to be assumed for 3D problems to obtain the coefficient of κ in Equation(7) during the calculation of the SEDF. However, it is sometimes rather intricate to simplify complex 3D problems into ideal plane state ones.

In order to solve the above two problems related to SEDF, a new approach named “element strain energy density (ESEDF) approach” based on FE analysis is proposed in this paper to realize the goal of direct computation of the SEDF and easy access to solution to fatigue crack growth problems. It is able to skip both the assumption of plane stress/strain state for 3D problems and the intricate step of calculating SIFs, for it directly computes the SEDF from FE analysis results. Cases of Mode I, Mode II, Mode III and mixed mode cracks are all discussed using both 2D and 3D FE models. The effect of mesh sizes on accuracy and the trade-off analysis to balance accuracy with computational cost are also discussed. Moreover, A da/dN-ΔS-R equation with consideration of stress ratios for mode I cracks is proposed and material constants were obtained by fitting of fatigue crack growth test data of CT specimens.

2 METHODOLOGY

The proposed ESEDF approach is based on the definition of SED ω itself, which is the total strain energy stored per unit volume, as shown in Equation (13):

$$S = \omega \cdot r = \lim_{\Delta V=0} \frac{\Delta W_t}{\Delta V} \cdot r = \frac{dW_t}{dV} \cdot r \tag{13}$$

where ΔW_t is the total strain energy within a volume of ΔV. When the volume is very small and infinitely close to 0, the SEDF S of the desired location is thus calculated according to Equation (13). Therefore, the meshing in the FE analysis model around the crack tip needs to be very refined to obtain the accurate SEDF S of the crack tip. Thus, a row of refined-meshed sector-shaped elements is normally generated around the crack tip during the meshing of the FE model. Singular elements, i.e., the mid-nodes of the quadratic sector elements around the crack tip are skewed to the 1/4 point, are required as shown in Figure 1(b). One of the sector-shaped elements is taken as an example as shown in Figure 1(a). Since the sector angle $\Delta\vartheta$ can be very small during the meshing, the SED ω of the element is assumed constant in the circumferential direction. It means that the SED of the location from ϑ to ϑ+$\Delta\vartheta$ in this sector element keeps unchanged (ϑ is the directional angle). The SED $\omega(\theta, r)$ within this sector element is expressed as Equation (14) according to Sih (1974)'s theory.

$$\omega(\theta, r) = S(\theta)/r \tag{14}$$

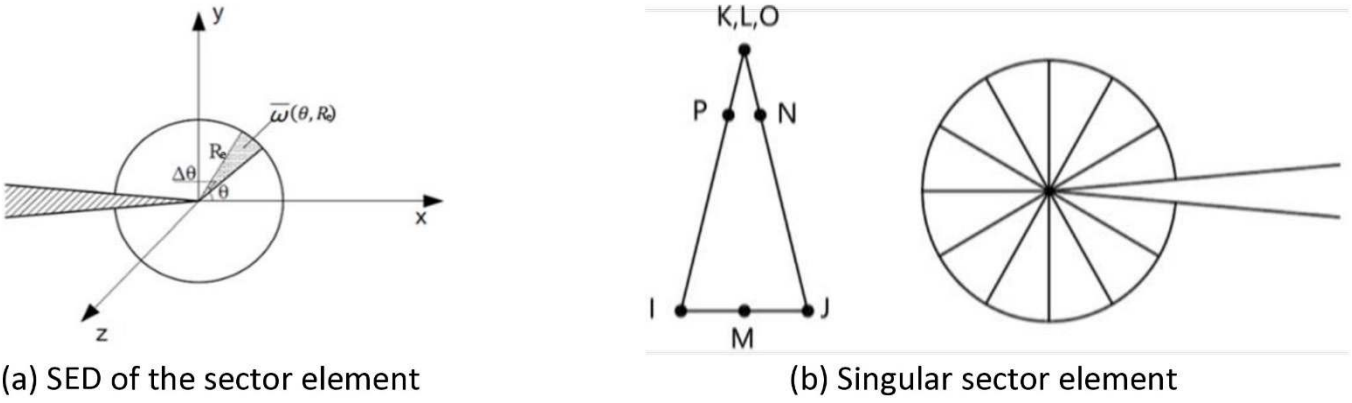


Figure 1 Sector elements around the crack tip

Thus, the total strain energy value W_t within this sector element with a sector angle of $\Delta\vartheta$ and a radius of R_e is obtained by the integration process using the SED value $\omega(\theta, r)$ at each location within this element as shown in Equation (15).

$$W_t(\theta, R_e) = \int_0^{R_e} \omega(\theta, r)\, r\Delta\theta dr = S(\theta) R_e \Delta\theta \tag{15}$$

The sector element volume V is expressed as Equation (16) since the sector angle $\Delta\vartheta$ is very small, where t is the sector element thickness.

$$V = 0.5 {R_e}^2 t\Delta\theta \tag{16}$$

Thus, the average SED of this sector element $\overline{\omega}(\theta, R_e)$ is expressed as Equation (17).

$$\overline{\omega}(\theta, R_e) = W_t(\theta, R_e)/V = 2S(\theta)/(R_e t) \tag{17}$$

Therefore, the SEDF within this sector element is shown as Equation (18) both for 3D models and 2D models if t is taken as one unit.

$$S(\theta) = \begin{cases} \bar{\omega}(\theta, R_e) \cdot \frac{R_e t}{2} & \text{3D} \\ \bar{\omega}(\theta, R_e) \cdot \frac{R_e}{2} & \text{2D} \end{cases} \tag{18}$$

Equation (18) is the core equation of the ESEDF approach. It indicates that the SEDF $S(\vartheta)$ in different directional angle ϑ at the crack tip can be obtained by the multiplication of half of the sector radius $R_e/2$ and the average SED $\bar{\omega}(\theta, R_e)$ within this element, as illustrated in Figure 1(a)(b), as long as a reasonable element radius R_e and a sector angle $\Delta\vartheta$ at the crack tip are defined for each sector element. The average SED can be directly abstracted from the FE analysis results without the assumption of a plane stress/strain state for a 3D problem and thus avoid the limitation of Sih's theory. From the above description, it is clear that the proposed ESEDF approach is classified as a local-fracture-parameter-extraction method, indicating that it is based on the local ESEDF results extracted from the crack tip. Due to this property, it has several advantages and limitations, which will all be discussed in the following sections.

3 DEMONSTRATION OF APPLICATION BY FE ANALYSIS

3.1 Mode I crack

To demonstrate the application of the ESEDF approach in a mode I crack problem, an infinitely large steel plate with a through crack with a length of 2*a*=10mm at the center was illustrated in Figure 2(a). The mechanical properties of the steel were that the elastic modulus was 210 GPa, Poisson's ratio was 0.3, the density was 7.85 g/cm^3, the yield strength was 321 MPa, which will be used in all the cases in this section. A tensile pressure equal to σ=0.06MPa was exerted on the top and bottom surfaces of the plate. Only 1/4 of the plate was focused on and the 2D FE model with a dimension 100mm×100mm×20mm was established using PLANE183, a 2-D 8-node or 6-node structural solid element, in the commercial software ANSYS. A symmetric boundary condition was assumed as shown in Figure 2(b). Rows of sector elements were generated using singular elements around the crack tip during the meshing. The sector angle $\Delta\vartheta$ was taken as 10° and the radius R_e was taken as 0.001mm for the first row of sector elements. Both the plane stress state and the plane strain state were considered respectively for the 2D model. To further demonstrate the approach in 3D FE models, a 3D model was established using SOLID186, a 3D 20-node structural solid element, as shown in Figure2(c). The boundary condition was almost the same as that of the 2D model. The mesh patterns near the crack tip for all the above models were illustrated in Figure2(d)(e).

The theoretical solution of the SIF for a mode I crack in an infinitely large plate was approximately applicable, as shown in Equation (19) summarized by Lawn and Wilshaw (1993) and the SEDF was given in Equation (20). The SEDF at the crack tip was calculated first by the indirect approach from the SIF (the SEDF approach by Sih), as Equation (20).

$$K_{\mathrm{I}} = \sigma\sqrt{\pi a} \tag{19}$$

$$S_{\mathrm{I}} = a_{11} K_{\mathrm{I}}^2 = \frac{K_{\mathrm{I}}^2}{16\pi G}(1 + cos\theta)(\kappa - cos\theta) \tag{20}$$

The indirect calculation with conventional SEDF approach was based on three FE computing methods, the displacement extrapolation, the interaction integral and J-Integral. The displacement extraction procedure is a conventional method to calculate SIF from nodal displacements of five nodes away from the crack tip, with one node at the origin and four other nodes on both crack faces. The equations are as shown in Equation(21) and Equation(22), where *u* and *v* are nodal displacement of these nodes, *r* and ϑ are the polar coordinates, K_{I} and K_{II} are SIFs under mode I and mode II cracks. The SIF is thus solved with the combination of these two equations. It is worth noting that displacement extrapolation is only limited to 2D FE models.

$$u = \frac{K_{\mathrm{I}}}{4G}\sqrt{\frac{r}{2\pi}}\left[(2k-1)\cos\frac{\theta}{2} - \cos\frac{3\theta}{2}\right] - \frac{K_{\mathrm{II}}}{4G}\sqrt{\frac{r}{2\pi}}\left[(2k+3)\sin\frac{\theta}{2} + \sin\frac{3\theta}{2}\right] \tag{21}$$

$$v = \frac{K_{\mathrm{I}}}{4G}\sqrt{\frac{r}{2\pi}}\left[(2k-1)\sin\frac{\theta}{2} - \sin\frac{3\theta}{2}\right] - \frac{K_{\mathrm{II}}}{4G}\sqrt{\frac{r}{2\pi}}\left[(2k+3)\cos\frac{\theta}{2} + \cos\frac{3\theta}{2}\right] \tag{22}$$

It is also able to calculate SIF from J-integral (known as *J* criterion), a parameter indicating a path-independent contour integration surrounding the crack tip, as shown in Eq(23). In the equation, Γ is the integration path around the crack tip, T_i is traction vector components, u_i is displacement vector components, ds is the length increment along the contour Γ.

$$J = \int_{\Gamma} \left(\omega(\theta, r)dy - T_i \frac{\partial u_i}{\partial x} ds\right) \tag{23}$$

The SIF is calculated by Eq(24) from J-integral.

$$K_1 = \sqrt{J \cdot E} \tag{24}$$

It is worth noting that it is difficult to deal with mixed mode cracks with J-integral and therefore the interaction integral was further introduced into the J-integral calculation. The idea of the interaction integral is based on J-integral, with interaction integral to separate SIF in mixed mode cracks. The interaction is to interact the real stress state (σ_{ij}, u_i) with an auxiliary stress state $(\sigma_{ij}^{aux}, u_{ij}^{aux})$ at the crack tip.

In addition to the indirect approach, the direct approach (the proposed ESEDF approach) was further adopted. The SIF *K* calculated by Equation (19) in the theoretical solution and that calculated by FE analysis in the SEDF approach were both further transformed into SEDF *S* by Equation (20) for both the above two approaches. In contrast, the SEDF was directly calculated by Equation (18) using FE analysis results in the ESEDF approach.

The minimum SEDF results within the first row of sector elements around the crack tip calculated by the above-mentioned numerical solutions and theoretical solutions were all listed in Table 1. It is worth noting that the displacement extrapolation is only limited in 2D FE analysis and thus the results of it in 3D models are not available in all the cases. It is found that the results of two numerical approaches are both very close to the theoretical solution with an error of less than 1%. The error of the SEDF approach based on different calculation procedure were relatively near to each other, while that of the ESEDF is far less than those of SEDF results, showing greater accuracy in mode I cracks.

3.2 Mode II crack

Mode II cracks also widely exist in engineering. The same infinitely large steel plate with a through crack with the same length at the center was illustrated in Figure 3(a). A uniform shear stress τ= 0.06MPa was exerted at four lateral surfaces of the plate. The theoretical solution of the SIF for a mode II crack in an infinitely large plate was approximately applicable as shown in Equation (25) summarized by Lawn and Wilshaw (1993) and the SEDF was obtained by Equation (26).

$$K_{\mathrm{II}} = \tau\sqrt{\pi a} \tag{25}$$

$$S_{\mathrm{II}} = a_{22}K_{\mathrm{II}}^2 = \frac{K_{\mathrm{II}}^2}{16\pi \mathrm{G}}[(k+1)(1-\cos\theta) + (1+\cos\theta)(3\cos\theta - 1)] \tag{26}$$

The same FE model of 1/4 of the plate was established using PLANE183 in ANSYS and an anti-symmetry boundary condition was assumed as shown in Figure 3(b). The same mesh pattern was adopted around the crack tip as shown in Figure2(d)(e). Both plane strain state and plane stress state were considered. An additional 3D model was also established using SOLID186 as shown in Figure 3(c). The sector angle $\Delta\vartheta$ was taken as 10° and the radius R_e was taken as 0.001mm. The results based on all the procedures were all listed in Table 1. It is found that the results are similar to those of the mode I crack. The results of the numerical solutions are both very close to the theoretical solution with an error of less than 1% and the error of the ESEDF approach is much less than the SEDF approach.

Table 1 Minimum SEDF results of a single mode crack

Case	Model	Parameter	ESEDF approach	SEDF approach			Theoretical solution
				Displacement extrapolation	Interaction integral	J-integral	
Mode I	2D-Plane strain	K_I (MPa·m$^{1/2}$)	-	7.550×10^{-3}	7.546×10^{-3}	7.546×10^{-3}	7.520×10^{-3}
		S_{min} (N/m)	2.229×10^{-5}	2.246×10^{-5}	2.244×10^{-5}	2.244×10^{-5}	2.229×10^{-5}
		J (N/m)	-	-	-	2.468×10^{-4}	2.450×10^{-4}
		Error of S_{min} %	0.03	0.76	0.67	0.67	-
	2D-Plane stress	K_I(MPa·m$^{1/2}$)	-	7.544×10^{-3}	7.546×10^{-3}	7.546×10^{-3}	7.520×10^{-3}
		S_{min} (N/m)	2.996×10^{-5}	3.019×10^{-5}	3.021×10^{-5}	3.021×10^{-5}	3.000×10^{-5}
		J (N/m)	-	-	-	2.712×10^{-4}	2.693×10^{-4}
		Error of S_{min} %	0.13	0.63	0.70	0.70	-
	3D	K_I(MPa·m$^{1/2}$)	-	-	7.549×10^{-3}	7.546×10^{-3}	7.520×10^{-3}
		S_{min} (N/m)	2.224×10^{-5}	-	2.246×10^{-5}	2.244×10^{-5}	2.229×10^{-5}
		J (N/m)	-	-	-	2.468×10^{-4}	2.450×10^{-4}
		Error of S_{min} %	0.22	-	0.76	0.67	-
Mode II	2D-Plane strain	K_{II}(MPa·m$^{1/2}$)	-	7.531×10^{-3}	7.532×10^{-3}	7.531×10^{-3}	7.520×10^{-3}
		S_{min} (N/m)	5.582×10^{-5}	5.587×10^{-5}	5.589×10^{-5}	5.589×10^{-5}	5.571×10^{-5}
		J (N/m)	-	-	-	2.458×10^{-4}	2.450×10^{-4}
		Error of S_{min} %	0.20	0.29	0.32	0.32	-
	2D-Plane stress	K_{II}(MPa·m$^{1/2}$)	-	7.530×10^{-3}	7.532×10^{-3}	7.531×10^{-3}	7.520×10^{-3}
		S_{min} (N/m)	5.583×10^{-5}	5.587×10^{-5}	5.589×10^{-5}	5.588×10^{-5}	5.571×10^{-5}
		J (N/m)	-	-	-	2.701×10^{-4}	2.693×10^{-7}
		Error of S_{min} %	0.21	0.28	0.32	0.31	-
	3D	K_{II}(MPa·m$^{1/2}$)	-	-	7.532×10^{-3}	7.565×10^{-3}	7.520×10^{-3}
		S_{min} (N/m)	5.578×10^{-5}	-	5.589×10^{-5}	5.639×10^{-5}	5.571×10^{-5}
		J (N/m)	-	-	-	2.480×10^{-4}	2.450×10^{-4}
		Error of S_{min} %	0.12	-	0.32	1.22	-
Mode III	3D	K_{III}(MPa·m$^{1/2}$)	-	-	7.549×10^{-3}	7.479×10^{-3}	7.549×10^{-3}
		S_{min} (N/m)	5.871×10^{-5}	-	5.542×10^{-5}	5.512×10^{-5}	5.571×10^{-5}
		J (N/m)	-	-	-	3.463×10^{-4}	3.501×10^{-4}
		Error of S_{min} %	5.40	-	0.50	1.06	-
Surface crack	3D	K_I(MPa·m$^{1/2}$)	-	-	1.252	1.233	1.254
		S_{min} (N/m)	0.599	-	0.635	0.611	0.632
		J (N/m)	-	-	-	6.720	6.946
		Error of S_{min} %	5.22	-	0.47	3.32	-

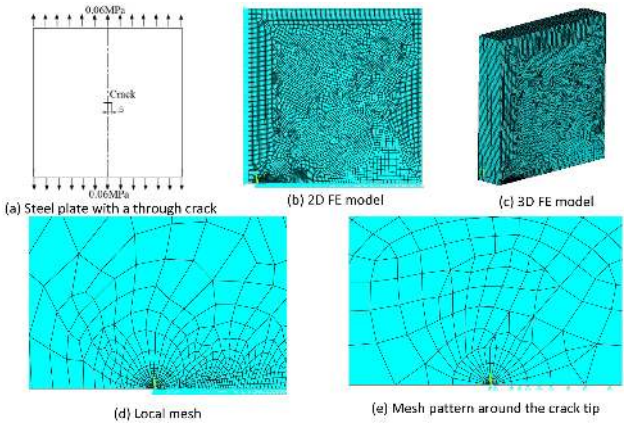


Figure 2 Mode I crack problem

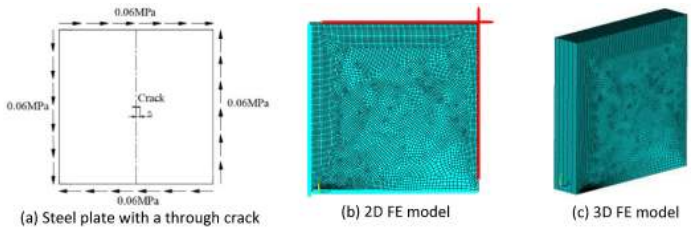


Figure 3 Mode II crack problem

3.3 Mode III crack

A mode III crack is also common in engineering and thus an infinitely large steel block with a through crack with a length of 2a=10mm at the center was illustrated in Figure 4(a). A uniform shear stress τ= 0.06MPa was exerted at four (top, bottom, front, and back) surfaces of the block. Half of the model was established by SOLID186 in ANSYS with a dimension of 200mm×100mm×200mm, with an angle $\Delta\vartheta$ of 11.25° and a radius R_e of 0.2mm for the first row of prism elements (3D) around the crack front, as shown in Figure 4(b)(c). The SEDF was calculated by both ESEDF approach and SEDF approach. The theoretical solution of the SIF for a mode III crack in an infinitely large block was approximately applicable, as shown in Equation (27) summarized by Lawn and Wilshaw (1993), and the SEDF was obtained by Equation (28).

$$K_{\mathrm{III}} = \tau\sqrt{\pi a} \tag{27}$$

$$S_{\mathrm{III}} = a_{33}K_{\mathrm{III}}^2 = \frac{K_{\mathrm{III}}^2}{4\pi \mathrm{G}} \tag{28}$$

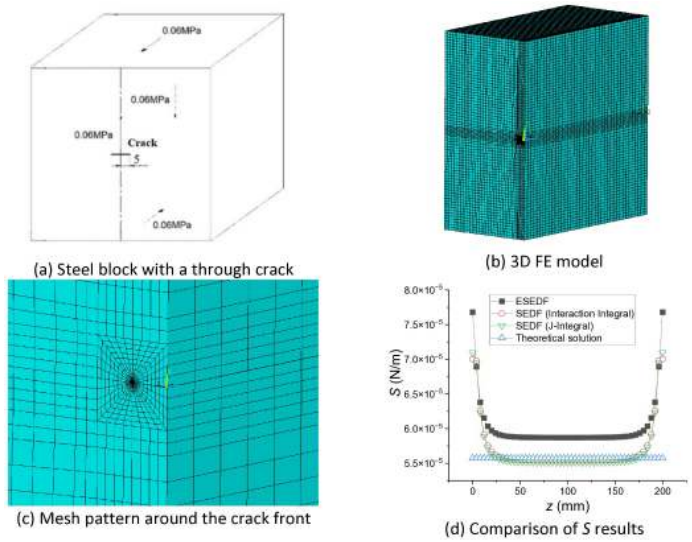


Figure 4 Mode III crack problem

The distribution of SEDF results along the crack front was plotted in Figure 4(d). It is found that the SEDF tends to be larger on the two lateral surfaces of the block than that within the block. The SEDF results at the center of the crack front with maximum error for the ESEDF approach were listed in Table 1. It reveals that both the numerical results are still very close to the theoretical results with an error of less than 6% while the error of the ESEDF approach is more than that of the SEDF approach, unlike in mode I and mode II crack cases. The reason will be systematically discussed in Section 4.

3.4 Surface crack

The above discussion is limited to cases of a through crack. However, a surface crack also frequently happens in engineering, for the engineering component surface is more exposed to manufacture imperfections and environmental corrosion. Thus, a surface crack problem is discussed. A steel block with a width of 72mm, a height of 80mm, and a thickness of 50mm was demonstrated as shown in Figure 5(a). Half FE model was established and a symmetric boundary

condition was assumed as shown in Figure 5(b). A 3D surface crack as half of a circle with a radius of 5mm was assumed and the crack length was 2a=10mm. The angle $\Delta\vartheta$ was taken as 18° and the radius of the first row of prism elements R_e was taken as 0.33mm as shown in Figure 5(c). A tensile pressure equal to σ=15MPa was exerted on the top and the bottom of the block, which made this case mainly belong to a mode I crack problem.

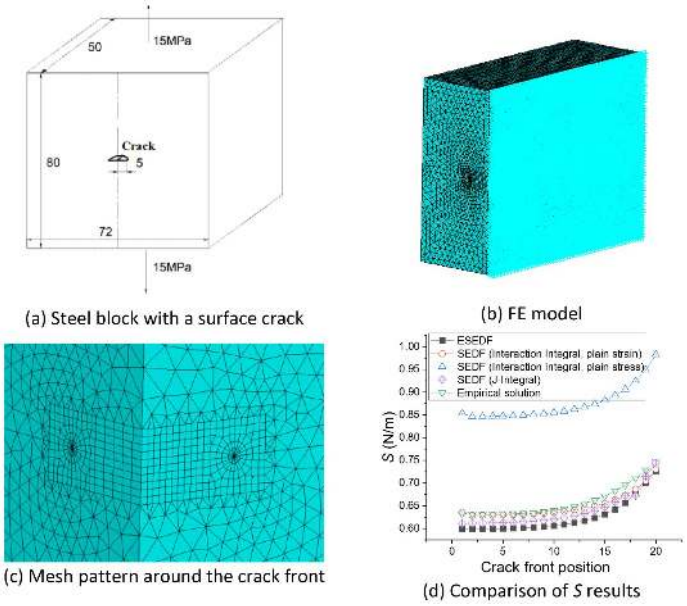


Figure 5 Case of a 3D surface crack

The groups of SEDF results along the crack front calculated by SEDF approach including plane stress state and plane strain state based on interaction integration, plain strain state based on J-integral, ESEDF approach, and empirical solution by Newman and Raju (1981) were illustrated respectively in Figure 5(d). It is found that the SEDF results by the SEDF approach under plane stress state assumption vary greatly from the other three groups of results. It indicates that this steel block is more likely to be under plane strain state rather than plane stress state. Therefore, the plane stress state was not discussed for J-integral in this case. Similar to the mode III crack case discussed above, the SEDF results tend to be larger on the surface of the block (Position 20) than that within the block (Position 1) and the error of the ESEDF approach is greater than the SEDF approach in most positions along the crack front. The error of the ESEDF approach at the node with symmetric boundary condition at the crack front (inner part of the block) was listed in Table 1, where plain strain state is assumed. It is found that numerical results are both very close to the empirical solution with an error of less than 6%. Similar to the above case with a mode III crack, the error of the ESEDF approach is more than that of the SEDF approach.

3.5 Mixed mode crack

A mixed mode crack problem is much more complex than a single mode one. An infinitely large steel plate was chosen for the demonstration. An oblique crack with a length of 2a=20mm and an inclination angle β of 45° was located at the center of the plate. A tensile stress σ=0.06MPa was exerted at both ends of the plate as shown in Figure 6(a) and this case was a mixed mode I-II crack problem. Both the 2D models (under plane stress state or plane strain state) and the 3D model were established in ANSYS with a dimension of 200mm×400mm×20mm as illustrated in Figure 6(b). A row of singular sector elements with a sector angle $\Delta\vartheta$ of 6° and a sector radius R_e of 0.001mm were generated around the crack tip as illustrated in Figure 6(c)(d). The other locations away from the crack tip were meshed by coarser mesh with a mesh size of 3mm.

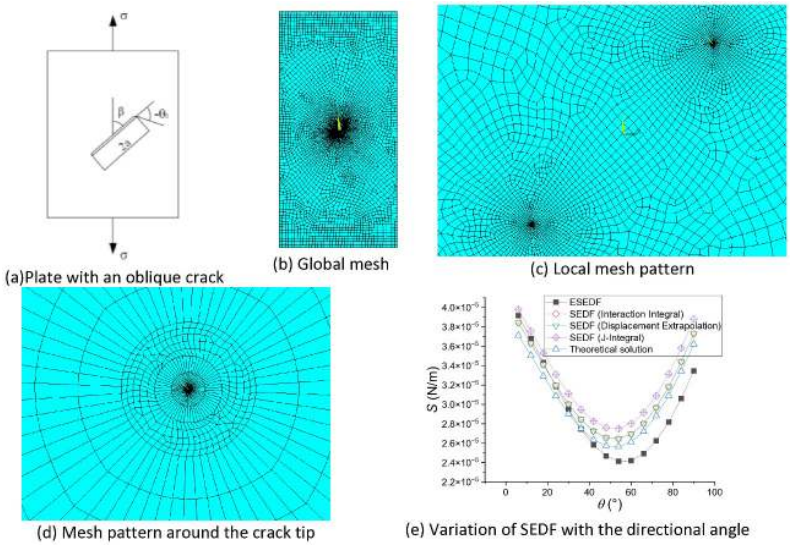


Figure 6 Plane oblique crack problem

The theoretical solution of the SIF for a mixed mode I-II crack in an infinitely large plate was approximately applicable as shown in Equation (29) and Equation (30).

$$K_{\mathrm{I}} = \sigma\sqrt{\pi a}\sin^2\beta \tag{29}$$

$$K_{\mathrm{II}} = \sigma\sqrt{\pi a}\sin\beta\cos\beta \tag{30}$$

According to the maximum circumferential stress criterion, the initial crack growth angle ϑ_0 should meet the following requirement as Equation (31) by Erdogan and Sih (1963):

$$\sin\theta_0 + (3\cos\theta_0 - 1)\cot\beta = 0, \beta \neq 0 \tag{31}$$

The theoretical solution of the SEDF could be calculated by Equation (32).

$$S = \sigma^2\pi a(a_{11}\sin^2\beta + 2a_{12}\sin\beta\cos\beta + a_{22}\cos^2\beta)\sin^2\beta \tag{32}$$

In a mixed mode crack problem, it is assumed that the crack will propagate in the direction with the minimum SEDF around the crack tip proposed by Sih (1974). The crack growth angle ϑ_0 and the minimum SEDF $S_{\min}$ were both calculated by SEDF approach and ESEDF approach. In addition to that, a theoretical solution was also given summarized by Erdogan and Sih (1963). The variation trend of the SEDF with the directional angle -ϑ for 2D-plane strain state was depicted in Figure 6(e). It is found that the SEDF changes considerably with the directional angle and a minimum SEDF is reached when $\vartheta \approx 54°$ for all the approaches and the theoretical solution.

The detailed information of minimum SEDF results around the crack tip were listed in Table 2, including 2D plane strain state, 2D plane stress state and 3D state. It is found that the SEDF and the crack growth angle results obtained by ESEDF approach and SEDF approach were both very close to the theoretical solution and the errors were less than 6%. Generally speaking, the error of the ESEDF approach is more than that of the SEDF approach, but it is not strictly followed.

4 EFFECT OF MESH PATTERN

It is widely known that mesh sizes around the crack tip affect the results in FE analysis of fracture mechanics. Therefore, the influence of mesh sizes on SEDF results by ESEDF approach needs to be discussed. Only the mode I crack problem is discussed in this section since it is the most common crack type. Mesh sizes including the sector angle and the sector radius for 2D models and also the prism height for 3D models are all discussed.

Table 2 Minimum SEDF results of mixed mode cracks

Condition	Model	Parameter	ESEDF approach	SEDF approach			Theoretical solution
				Displacement extrapolation	Interaction integral	J-integral	
Mixed mode (Plane Oblique Crack)	2D-Plane strain	Crack growth angle (ϑ_0)	54°	54°	54°	54°	53.1°
		K_I (MPa·m$^{1/2}$)	-	5.364×10^{-3}	5.359×10^{-3}	5.505×10^{-3}	5.317×10^{-3}
		K_{II} (MPa·m$^{1/2}$)	-	5.429×10^{-3}	5.417×10^{-3}	5.505×10^{-3}	5.317×10^{-3}
		S_{min} (N/m)	2.413×10^{-5}	2.646×10^{-5}	2.645×10^{-5}	2.749×10^{-5}	2.565×10^{-5}
		J (N/m)	-	-	-	2.390×10^{-4}	2.450×10^{-4}
		Error of S_{min} (%)	5.90	3.16	3.10	7.17	-
	2D-Plane stress	Crack growth angle (ϑ_0)	54°		54°	54°	53.1°
		K_I (MPa·m$^{1/2}$)	-	5.437×10^{-3}	5.364×10^{-3}	5.571×10^{-3}	5.317×10^{-3}
		K_{II} (MPa·m$^{1/2}$)	-	5.445×10^{-3}	5.395×10^{-3}	5.571×10^{-3}	5.317×10^{-3}
		S_{min} (N/m)	3.282×10^{-5}	3.417×10^{-5}	3.341×10^{-5}	3.582×10^{-8}	3.263×10^{-5}
		J (N/m)	-	-	-	2.690×10^{-4}	2.693×10^{-4}
		Error of S_{min} (%)	0.58	4.72	2.39	9.77	-
	3D	Crack growth angle (ϑ_0)	54°	-	54°	54°	53.1°
		K_I (MPa·m$^{1/2}$)	-	-	5.418×10^{-3}	5.541×10^{-3}	5.317×10^{-3}
		K_{II} (MPa·m$^{1/2}$)	-	-	5.505×10^{-3}	5.541×10^{-3}	5.317×10^{-3}
		S_{min} (N/m)	2.758×10^{-5}	-	2.711×10^{-5}	2.786×10^{-5}	2.565×10^{-5}
		J (N/m)	-	-	-	2.422×10^{-4}	2.450×10^{-4}
		Error of S_{min} (%)	7.52	-	5.69	8.62	-

4.1 Sector angle

The radius R_e of sector elements was kept to be 0.001mm and the sector angle $\Delta\vartheta$ was set to be some certain values from 6° to 20°. The SEDF was calculated using both singular elements and non-singular elements. A factor k was defined to be the quotient of the numerical SEDF result to the theoretical SEDF result and k should be near to 1 if both results agreed with each other. The results were all illustrated in Figure 7(a). It reveals that the results by ESEDF approach is not very sensitive to the variation of sector angle, since the factor k is 1.02 with an error of only 1.87% even when the sector angle is amplified to 20°. Moreover, it is obvious from Figure 7(a) that the results by non-singular elements deviate greatly from the theoretical solutions. It thus indicates that non-singular elements cannot be directly used in the ESEDF approach. The factor results of k keeps almost constant for the approaches based on SEDF, barely affected by the sector angle.

4.2 Sector radius

The sector angle $\Delta\vartheta$ was kept to be 10°, and the sector radius R_e was set to be some certain values from 0.001mm to 1mm. The factor results were illustrated in Figure 7(b). It is found that the factor k is relatively stable with the decrease in the sector radius R_e at first stage and begins to fluctuate from R_e=0.1mm for the SEDF approach based on displacement extrapolation, with a minimum k of 1.01 and an error of 0.8%, and a maximum k of 1.07 and an error of 7%. For ESEDF approach, the factor k continues to decrease with the increase in the sector radius, until the sector radius R_e reaches 0.5mm (knee point), with a k of 0.87 and a maximum error of 12.98%. It later begins to rise with gradually accelerated increasing rate and finally reaches 1.0003 with an error of only 0.03%. Moreover, the factor k keeps almost constant for SEDF approach based on interaction integral and J-integral, showing that both are much less sensitive to the variation of the sector radius. It indicates that the use of ESEDF approach is able to obtain more accurate results than the use of SEDF approach, provided that sufficiently refined meshes are guaranteed around the crack tip. Or else, it will lead to less accurate results than the use of SEDF approach.

4.3 Triangular prism height

The 3D model in Section 3.1 was selected to discuss the effect of the prism height Δt and the factor results were given in Figure 7(c). It is found that the SEDF does not change with the prism height for all the approaches. Therefore,

there is no special requirement for the mesh size along the crack front, as long as it makes elements to meet the aspect ratio requirement for all the cases.

4.4 Surface crack

The surface crack model in Section 3.4 was selected to discuss the mesh sensitivity in 3D models. It has been demonstrated that the results by ESEDF approach is more sensitive to the variation of the sector radius, thus the crack front of the model was meshed with a sector radius of 0.333mm, 0.01mm and 0.001mm, respectively. The results of the factor k were illustrated in Figure 7(d). It is found that the factor changes considerably with the decrease in the sector radius especially for the ESEDF approach. The error of results by ESEDF approach can reach less than 3% or less, with a sector radius $R_e \leq 0.001$mm, at the cost of tremendous increase in computational cost, especially for 3D large-scale complex models. On the other hand, the SEDF approach based on interaction integral can achieve more accurate SEDF results based on current mesh patterns, while the SEDF approach based on J-integral only achieves almost equivalent SEDF results with ESEDF approach.

4.5 Trade-off analysis

The above analysis reveals that the proposed ESEDF approach is extremely sensitive to the mesh patterns around the crack tip and thus tremendous numbers of nodes and elements sometimes are required for the computation of accurate ESEDF results. Therefore, a trade-off analysis is necessary to balance the need for accuracy and the computational cost.

It has been found that the ESEDF results are more sensitive to the variation of the sector radius and less sensitive to the change of the sector angle in both 2D and 3D models, while it is almost not affected by the change of the prism height in a 3D model. Therefore, the trade-off analysis for prism height will not be conducted. A mesh-refinement area shown as the two rows of semicircles containing sector elements in Figure 2(e) were chosen to conduct the trade-off analysis of the 2D model with a mode I crack. Detailed information of the model with various sector angles is given in Table 3, with the node and element number in the mesh-refinement area N_n and N_e, the radius of the mesh-refinement area R_d, the mesh density of the mesh-refinement area $D_e = N_e/(\pi \cdot R_d^2)$, total node number and element number in the model N_{nt} and N_{et}. The error of SEDF for the four approaches are also listed, including ER_{ESEDF} (ESEDF approach), $ER_{SEDF\text{-}DE}$ (SEDF approach by displacement extrapolation), $ER_{SEDF\text{-}II}$ (SEDF approach by interaction integral) and $ER_{SEDF\text{-}JI}$ (SEDF approach by J-integral). Moreover, the variation of errors and the mesh density D_e with that of the sector angle $\Delta\vartheta$ is illustrated in Figure 7(e). It is found from the table and the figure that a sector angle of 10° is able to obtain the most accurate result with satisfying computing resources cost, only about 2/3 of the cost for the case with a sector angle of 6°, in terms of the mesh density. This type of mesh pattern also meets the guide to the FE method, which suggests a sector of 10 degrees or less for the division of a circle. However, the sector angle can be allowed to at most 15° if a refined sector angle cannot be guaranteed in real large-scale engineering structures, which costs about half of the computing resources for the case with a sector angle of 10° and thus tremendously decreases the computational cost.

Table 3 Error and mesh density with sector angle for 2D mode I cracks

$\Delta\vartheta$ (°)	N_n	N_e	R_d (mm)	D_e (Elements/mm^2)	N_{nt}	N_{et}	ER_{ESEDF} (%)	$ER_{SEDF\text{-}DE}$ (%)	$ER_{SEDF\text{-}II}$ (%)	$ER_{SEDF\text{-}JI}$ (%)
6	1490	495	3.54×10^{-2}	1.26×10^{5}	375827	124632	0.295	0.776	0.700	0.696
9	1055	346	3.54×10^{-2}	8.81×10^{4}	377145	125052	0.079	0.733	0.691	0.700
10	922	303	3.54×10^{-2}	7.72×10^{4}	371698	123257	0.032	0.792	0.691	0.704
12	781	254	3.54×10^{-2}	6.47×10^{4}	368825	122280	0.303	0.700	0.691	0.700
15	560	179	3.54×10^{-2}	4.56×10^{4}	361522	119841	0.808	0.683	0.683	0.696
20	455	142	3.54×10^{-2}	3.62×10^{4}	369751	122586	1.870	0.641	0.683	0.696

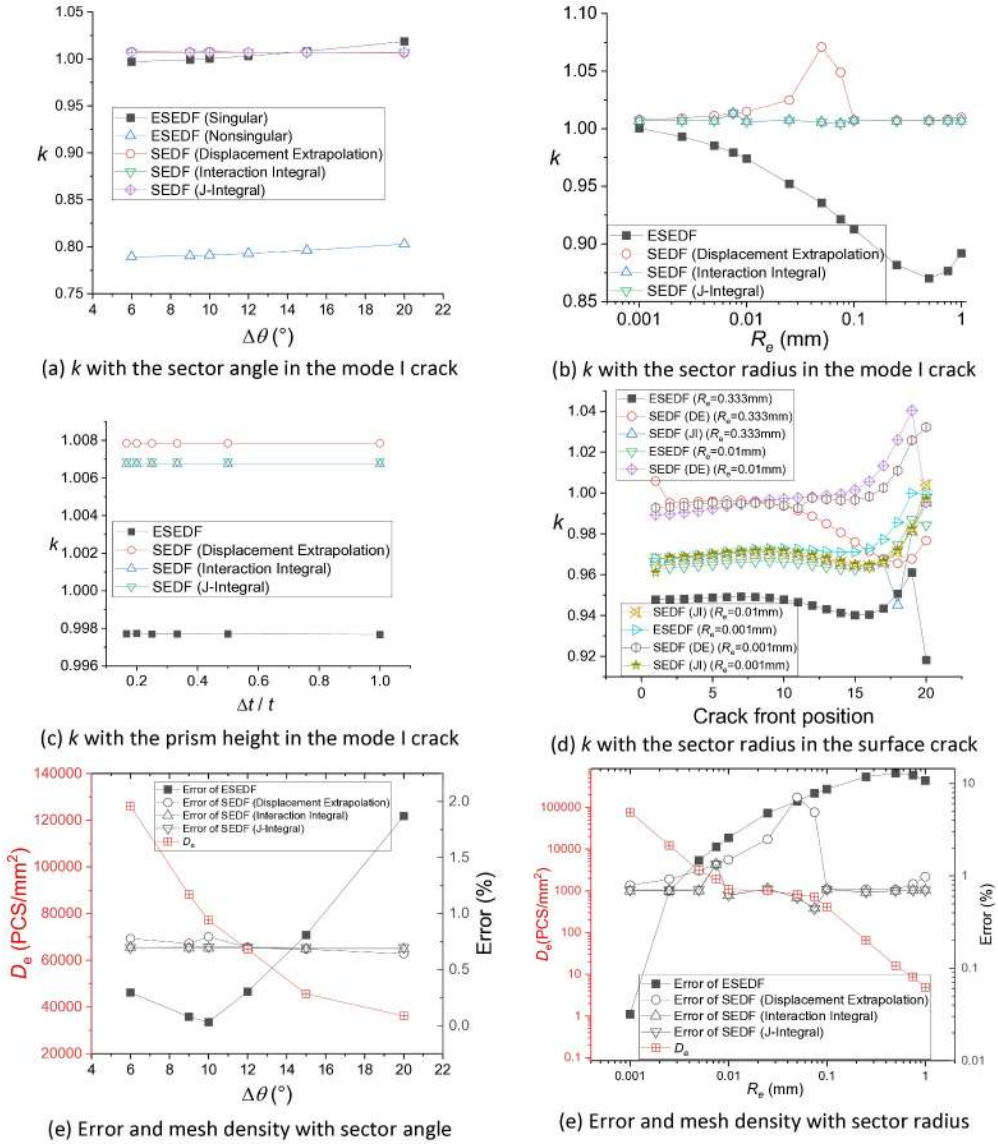


Figure 7 Effect of mesh sizes on the SEDF results

Table 4 Error and mesh density with sector radius for 2D mode I cracks

R_e (mm)	N_n	N_e	R_d (mm)	D_e (Elements/mm2)	N_{nt} (PCS)	N_{et} (PCS)	ER_{ESEDF} (%)	$ER_{SEDF-DE}$ (%)	$ER_{SEDF-II}$ (%)	$ER_{SEDF-JI}$ (%)
0.001	922	303	3.54×10^{-2}	7.72×10^{4}	371698	123257	0.032	0.792	0.691	0.704
0.0025	922	303	8.84×10^{-2}	1.23×10^{4}	64994	21399	0.686	0.919	0.691	0.704
0.005	922	303	1.77×10^{-1}	3.09×10^{3}	18494	6033	1.470	1.139	0.691	0.708
0.0075	830	271	2.12×10^{-1}	1.92×10^{3}	12681	4124	2.065	1.334	1.334	1.337
0.01	830	271	2.83×10^{-1}	1.08×10^{3}	7404	2391	2.591	1.494	0.615	0.623
0.025	438	141	2.12×10^{-1}	9.97×10^{2}	6293	2018	4.785	2.488	0.725	0.721
0.05	325	106	2.30×10^{-1}	6.39×10^{2}	5522	1777	6.436	7.085	0.581	0.582
0.075	326	105	2.65×10^{-1}	4.75×10^{2}	3814	1221	7.857	4.886	0.447	0.443
0.1	326	105	3.54×10^{-1}	2.67×10^{2}	4283	1370	8.720	0.716	0.716	0.717
0.25	494	159	8.84×10^{-1}	64.8	5142	1659	11.822	0.716	0.666	0.672
0.5	494	159	1.77	162	5033	1624	12.979	0.708	0.691	0.692
0.75	382	123	2.12	8.70	6893	2232	12.339	0.818	0.700	0.700
1	382	123	2.83	4.89	7601	2470	10.803	0.978	0.700	0.700

Table 5 Error and mesh density with sector radius for 3D surface cracks

R_e (mm)	N_n	N_e	V_d (mm^3)	D_e (Elements/mm^3)	N_{nt}	N_{et}	ER_{ESEDF} (%)	$ER_{SEDF\text{-}DE}$ (%)	$ER_{SEDF\text{-}II}$ (%)	$ER_{SEDF\text{-}JI}$ (%)
0.001	113141	29802	116	257	308260	169661	2.721	-	0.621	2.837
0.010	34981	9054	116	78	229703	148604	3.378	-	0.280	2.291
0.333	15325	3720	116	32	210537	143664	4.613	-	0.635	2.925

The detailed information of the model with different sector radius for the 2D model with a mode I crack is shown in Table 4 and Figure 7(e). It is worth noting that logarithmic coordinates are used in Figure 7(e) to better demonstrate the figure. It is clearly found that a sector radius of 0.001mm can lead to more accurate results for ESEDF approach than those by other approaches. Therefore, if the computing resource allows, a sector radius of 0.001mm is always recommended. However, balance should be kept if the computing resource is limited. It is found from Figure 7(e) that the mesh density decreases from 3.09×10^3 elements/mm^2 to 9.97×10^2 elements/mm^2, almost by 2/3, when the sector radius is increased from 0.005mm to 0.025mm and the error is increased from 1.470% to 4.785%, almost tripled. It means that the error is diminished by 2/3 with almost tripled amount of computational cost, which is absolutely worth it, compared with other cases. Moreover, compared with the original case with a sector radius of 0.001mm, the error only increases from 0.032% to 1.470% but the mesh density reduces from 7.72×10^4 elements/mm^2 to 3.09×10^3 elements/mm^2, indicating that the computational mesh density was reduced by approximately 25 times. Therefore, to utilize the above phenomenon, the sector radius is recommended to be 0.005mm for economical computational cost if a value of 0.001mm is not available. In addition, it is found that results with allowable error are still obtained with a maximum error of 10.803%, compared to the accurate 1.470%, even when the mesh size is amplified to 1mm. It can still meet the accuracy demands of engineering issues, especially real large-scale engineering structures with only 0.006% (4.89 elements/mm^2) of that in the case with a sector radius of 0.001mm (7.72×10^4 elements/mm^2) and saves considerable amount of computational cost.

Therefore, three levels of mesh recommendations can be thus established. A sector radius of 0.001mm is suggested to obtain accurate SEDF results for small-scale engineering specimens or components to achieve absolute accuracy. However, if the computational cost does not allow, a sector radius of 0.005mm is recommended to achieve economical computational cost which balances the cost with accuracy. Additionally, it can be even allowed to 1mm if refined mesh cannot be guaranteed in real large-scale engineering structures. Meanwhile, it is found that the results by SEDF approach based on three procedures are far less sensitive to the variation of the sector radius, especially for that based on interaction integral and J-integral. The main reason is that the ESEDF approach is based on first-row-element local extraction, while SEDF approach by interaction integral and J-Integral are based on averaged idea of integration, which can decrease the effect of mesh patterns to some extent. Therefore, the ESEDF approach is much more sensitive to the mesh patterns around the crack tip, which is a main limitation of the proposed ESEDF approach.

Last, the detailed information of the model with different sector radius for the 3D surface model is listed in Table 5. The sandwich-shaped mesh-refinement volume with a volume of V_d containing the surface crack front as shown in Figure 5(c) is focused on and the mesh density is defined as: $D_e = N_e/ (V_d)$. It is found that the error is increased by almost 25% twice (from 2.721% to 4.613%) when the sector radius is changed from 0.001mm to 0.010mm and then to 0.333mm, with mesh density decreased from 257 elements/mm^3 to 78 elements/mm^3 and to 32 elements/mm^3. It is found that the accuracy improvement from the refinement of meshes becomes less effective in 3D FE models. It indicates that the error sources in 3D fracture analysis are no longer dominated solely by mesh density around the crack tip, but are increasingly affected by additional factors such as crack-front curvature, free-surface effects, mode coupling, etc. Therefore, unlike 2D crack problems, excessively refined crack-tip meshes are not always computationally economical for 3D analysis. Therefore, from the view of mesh density, a sector radius of 0.010 mm is more economical if limited computing resource is involved. However, a sector radius of 0.333mm can still lead to satisfying SEDF results for 3D models with relative low demand of computing resources, resulting into an error less than 5%.

Generally speaking, it is recommended to use quadratic singular structural elements at the crack tip to create a row of sector (prism for 3D) elements with an angle of 10°, a radius of 0.001mm and a prism height which meets element aspect ratio requirement during the FE analysis to get accurate results for the ESEDF approach, while the mesh patterns are allowed to be sparser to an angle of 15° and a radius of 1mm if very refined meshes cannot

be guaranteed. Moreover, a sector radius of 0.333mm can be allowed in 3D FE models in real large-scale engineering structures.

4.6 Discussion

After the comparison between SEDF results by ESEDF approach, SEDF approach and theoretical or empirical solutions in the above series of cases, it is found that the use of the ESEDF approach generally achieves more accurate results in mode I and mode II crack problems for both 2D and 3D models. However, it achieves less accurate results in mode III crack problems, mixed mode crack problems and also surface crack problems. The reasons can be systematically explained as follows.

Reason (1): The ESEDF approach and the SEDF approach based on displacement extrapolation can both be classified as local-fracture-parameter-extraction methods. The difference between them is that the former is based on first-row-element local extraction of SED with stronger singularity ($\omega \sim 1/r$) while the latter is based on local extraction of displacement with weaker or even non-singularity ($u \sim r^{1/2}$). It results into more sensitivity of ESEDF to mesh qualities around the crack tip. Meanwhile, since the SEDF varies in different direction around the crack tip (front), normally only one single sector element is involved in the SEDF extraction for the former, which amplifies the potential chance of error. Therefore, the latter is thus less sensitive to the variation of mesh sizes. In addition, the SEDF approach by interaction integral and J-integral are both based on averaged idea of integration and the error is offset more by contour averaging and area integration. It thus results into their less sensitivity to mesh sizes, compared with ESEDF approach and SEDF approach based on displacement extrapolation. In general, refined mesh is relatively easy to achieve for 2D models but difficult for complex 3D models. For example, the accuracy of the ESEDF approach increases much more when the mesh size is refined from 0.01mm to 0.001mm compared with that when the mesh size is refined from 0.333mm to 0.01mm in the case of the surface crack model. The accuracy may continue to increase with further refined meshes but it is difficult to realize in real engineering cases.

Reason (2): The better accuracy performance of the ESEDF approach in 3D mode I and mode II crack problems mainly stem from the fact that the ESEDF approach directly calculates the SEDF from the FE analysis results without relying on plane stress/strain assumptions or SIF derivation. Thus, it is capable of obtaining the actual 3D crack-front constraint effects more directly than the conventional SEDF approach in relatively regular 3D crack problems. However, the crack-front stress or strain fields become significantly more complex due to anti-plane shear deformation, crack-front curvature, free-surface effects and mixed-mode coupling for 3D mode III cracks, surface cracks and mixed mode cracks. Therefore, the local SED field near the crack front varies much more drastically and becomes highly sensitive to local mesh sizes. Moreover, the ESEDF approach directly extracts the SED from both stress and strain fields in the singular crack-front elements and thus local numerical errors tend to accumulate and be amplified more significantly. In contrast, the conventional SEDF approach based on three methods involves domain integration or asymptotic field fitting processes, which provide certain averaging and smoothing effects. Therefore, the proposed ESEDF approach can achieve more accurate results in 2D or 3D single mode crack problems for FE models with simple crack tip (front) geological configurations (mode I or mode II cracks) while less accurate results in 3D single mode crack or mixed mode crack problems for FE models with complex geological configurations (mode III, surface crack or mixed mode cracks).

Reason (3): There is no proper theoretical solution for 3D models in some cases. For example, an empirical solution was used in the case of the block with a surface crack for comparison but it was by no means a theoretical one and its accuracy was still not absolutely definite. In the case of the plate with a mixed mode I-II crack, the theoretical solution itself was based on plane state so that there would be inevitable error when it was applied to a 3D model.

Based on the above analysis, the applicable domain of the proposed ESEDF approach can be thus summarized. It is clear that the ESEDF approach is most suitable to mode I crack problems, mode II crack problems, 2D crack problems, 3D crack problems with simple crack front configurations along with sufficiently refined crack-front mesh, and situations without explicit plane stress/strain assumptions, since it can achieve more accurate results without the definition of plane stress/strain assumptions, compared with the conventional SEDF approach. Meanwhile, it is less accurate in 3D mode III crack problems, complex 3D mixed-mode crack problems and engineering models with coarse meshing, though it is still with acceptable accuracy.

Moreover, it is worth noting that the displacement extrapolation method is not available for 3D FE models and thus the interaction integration and the J-integral are the only two methods available for the conventional SEDF approach in 3D models. In most cases with single mode cracks with simple crack tip (front) geological configurations, the results by these two methods are almost the same. However, for 3D models with complex geological crack front or mixed mode cracks, SEDF approach based on interaction integration can achieve more accurate results than SEDF approach based on J-integral. This is due to the fact that interaction integration is based on the interaction between the actual stress field

and the auxiliary stress field at the crack tip in addition to the simple integration and thus decrease the potential error more. Therefore, it is concluded that interaction integration is the best option among all the three options mentioned in this paper for conventional SEDF approach.

5 ESEDF APPROACH IN FATIGUE CRACK GROWTH ANALYSIS CONSIDERING THE STRESS RATIO

In general, the conventional fatigue crack growth assessment based on SEDF approach is conducted by Equations (8)(10) or Equation (11) to consider the effect of stress ratio, however, in the form of SIF range and SIF mean value in Equation(10). Therefore, the above equation is not applicable to the proposed ESEDF approach since the calculation of SIFs is skipped in this approach. Regarding to Equation(11), there are totally seven constants needed to obtain from fitting to experimental data and it seems too tedious. Thus, it is necessary to develop a proper and simple fatigue crack growth assessment equation for the proposed ESEDF approach.

The famous Paris law without the consideration of the stress ratio effect is shown in Equation (33),

$$\frac{da}{dN} = C_p(\Delta K)^{m_p} \tag{33}$$

where C_p and m_p are constants based on materials, ΔK is the SIF range and it is:

$$\Delta K = K_{\max} - K_{\min} \tag{34}$$

Later, Walker considered the stress ratio effect in Paris law and modified Equation (34) into Equation (35) by Walker (1970),

$$\frac{da}{dN} = C_0\left(\frac{\Delta K}{(1-R)^{1-\gamma}}\right)^{m_0} \tag{35}$$

where C_0, m_0 and γ are constants dependent on materials; *R* is the stress ratio and it is:

$$R = K_{\min}/K_{\max} \tag{36}$$

Thus, according to Equation (20), Equation (34) and Equation (36), Equation (35) is further derived into Equation (37) and it is named as d*a*/d*N*-Δ*S*-*R* equation to consider the stress ratio effect,

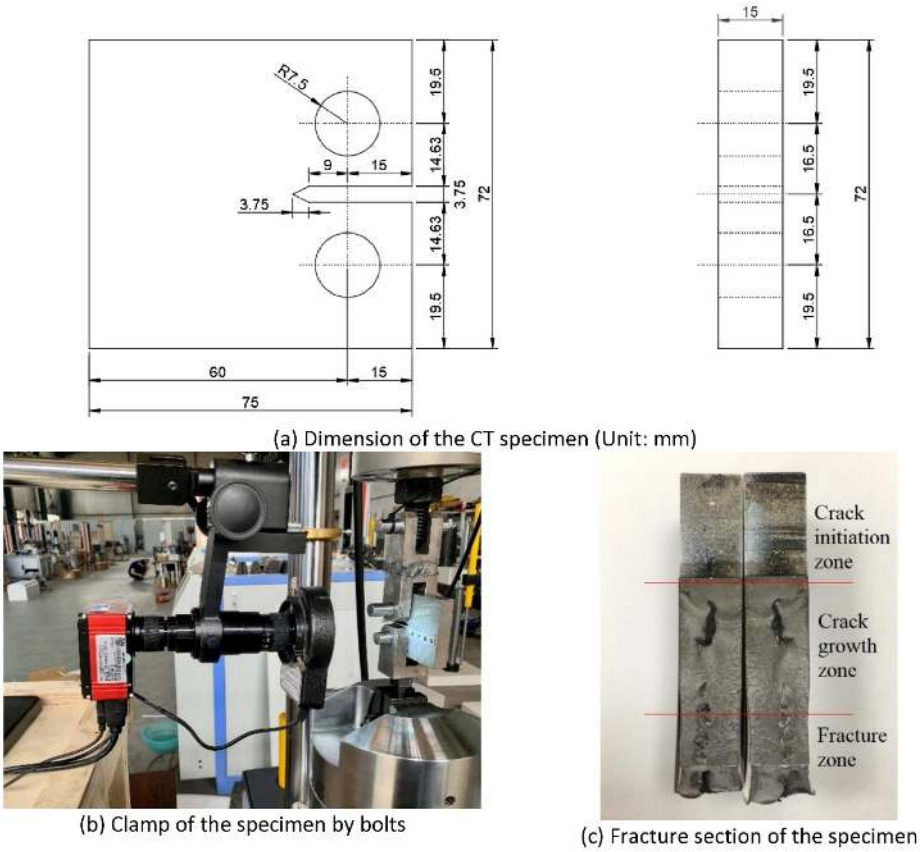
$$\frac{da}{dN} = C_0\left(\frac{\Delta S(1-R)^{2\gamma-1}}{a_{11}(1+R)}\right)^{\frac{m_0}{2}} \tag{37}$$

where C_0, m_0 and γ in Equation (37) are the same material-dependent constants as those in Equation (35) and they can be obtained by fitting to fatigue tests results of CT specimens. Since θ is 0 in the parameter of a_{11} for a mode I crack as shown in Equation (2), Equation (37) is further derived into Equation (38). However, it is worth noting that the proposed d*a*/d*N*-Δ*S*-*R* equation is only limited to mode I cracks because the above derivation is based on mode I cracks. Therefore, the following experimental research is also conducted on mode I fatigue crack growth.

$$\frac{da}{dN} = C_0\left(\frac{16\pi G\Delta S(1-R)^{2\gamma-1}}{(\kappa-1)(1+R)}\right)^{\frac{m_0}{2}} \tag{38}$$

The fatigue test of CT specimens made of structural steel GB Q235B and GB Q355B were conducted on a 100t high-frequency fatigue testing machine at room temperature. The carbon structural steel GB Q235B, approximated to EN S235JR, is with an elastic modulus of 179 GPa and a yield strength of about 321 MPa. The low alloy high strength structural steel GB Q355B, approximated to EN S355JR, is with an elastic modulus of 182 GPa and a yield strength of about 469 MPa. The CT specimens with a thickness of *B*=15 mm and a width of 1.25*W* (*W*=60 mm) were manufactured from a thin steel plate, as shown in Figure 8(a). A notch was manufactured at the center of the plate and two clamping holes for bolts were made near each side of the notch. The distance from the notch tip to the axis of the tensile load was marked as c_a=12.75mm. A crack with a length of a_p=5.75mm was prefabricated at the notch tip by a preloading procedure to

create a sharp straight crack with sufficient length to avoid the effect of the initial notch shape according to GB/T 6398-2017 (2017). A cyclic loading with a maximum force of F_{max}=37kN, a stress ratio of R=0.1 and a frequency of 30Hz was applied on all the specimens during the early pre-cracking stage, including fatigue initiation and fatigue crack growth, until the crack length reached a_p=5.75mm. When the crack length almost reached a length of a_p=5.75mm, the frequency was reduced to 1Hz for better observation of the crack length. Therefore, the initial crack length was considered as $a_0=a_p+c_a$ =18.5 mm with which the formal test started. The crack was classified as a mode I crack. The specimens were clamped at the ends between two steel plates fastened by bolts, as shown in Figure 8(b). The cyclic loading of sine waves with a frequency of 30 Hz was exerted through the two bolts and the loading patterns were listed in Table 6. The crack growth process for each specimen was divided into several growth steps and the crack length of each step was measured by a ruler stick on the specimen and a microscope, with the related number of cycles in each step being recorded as shown in Figure 8(b). The test was finished when the relative displacement between the two clamping ends reached 15mm.



(a) Dimension of the CT specimen (Unit: mm)

(b) Clamp of the specimen by bolts

(c) Fracture section of the specimen

Figure 8 Fatigue crack growth test

During the cyclic loading, fatigue cracks all initiated from the prefabricated crack and continued to grow along the center line. The macroscopic fracture section of one specimen was shown in Figure 8(c). It is found that the section was clearly divided into three areas: the prefabricated notch and the crack initiation zone, the crack growth zone, and the final failure zone.

It is worth noting that the proposed ESEDF approach for fatigue crack growth rate analysis is limited to the stable crack growth stage with a growth rate approximately from 10^{-6} to 10^{-2} mm/cycle in which the crack growth rate da/dN is in a straight line with the SEDF range ΔS in a log(da/dN) -logΔS coordinate, similar with the requirement of Paris law, summarized by Sih (1984). All the test data were within this stable crack growth stage.

The SEDF results of specimens in each crack growth step during the test was obtained from the finite element analysis results using the proposed ESEDF approach. The logarithm of SEDF ranges were correlated with that of the crack growth rate for all specimens as illustrated in Figure 9(a)(b) and it shows an approximately linear correlation with each other for all specimens under each stress ratio. The linear curve drops down in the figure with the increase of the stress ratio, indicating a faster crack growth rate. It proves that the fatigue crack growth rate is indeed affected greatly by stress ratios. The key parameters of log(C) and n for each group of specimens under each stress ratio in Equation (8) were obtained by the least square method and listed in Table 6. It is worth noting that the unit of SEDF range ΔS is MN/m and

that of SIF range ΔK is MPa·m$^{1/2}$ while that of the crack growth rate is m/cycle in the calculation of the parameters in Table 6. It is found that generally these two parameters increase as the stress ratio grows. The results were also compared with those obtained for the steel AISI 300M with a C of 1.656×10^{-3} (log(C)=-2.7809) and an n of 1.234 by Sih (1984) and it is found that the two constants are near to those for steel GB Q235B and GB Q355B in Table 6.

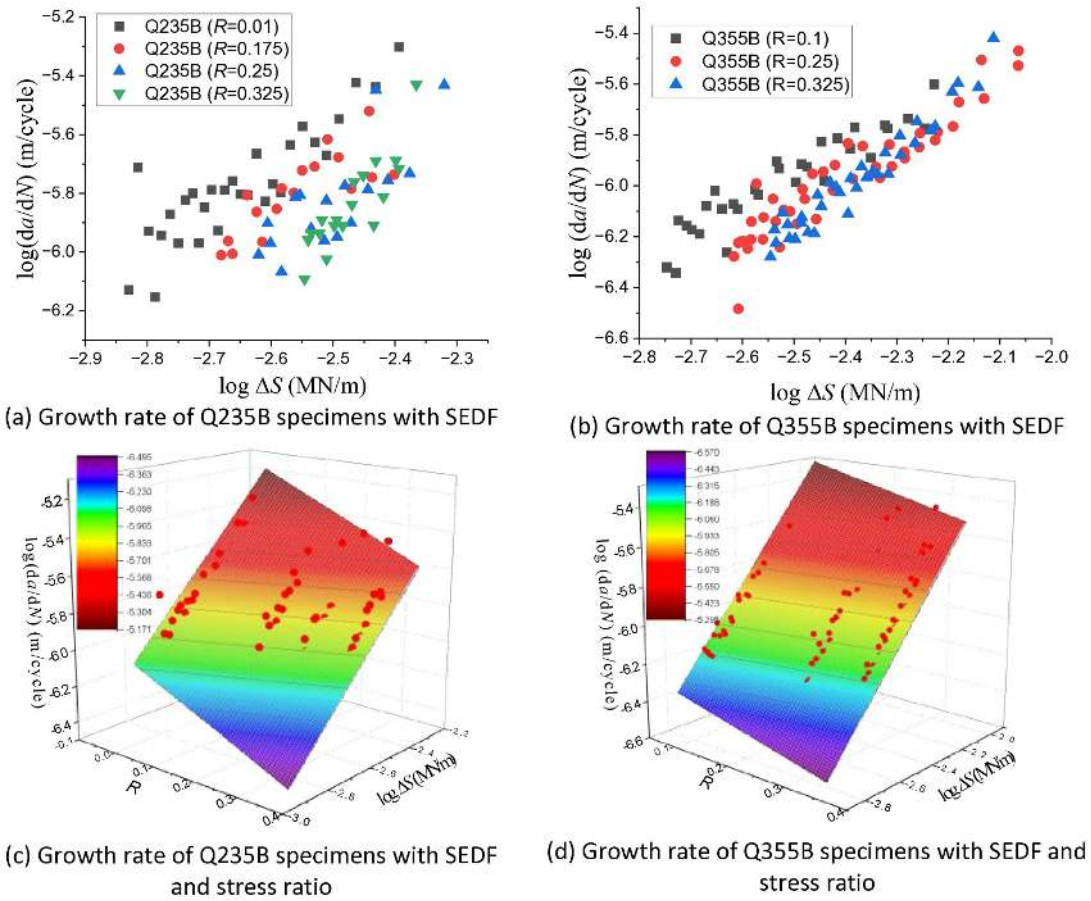


Figure 9 Fatigue crack growth test results of CT specimens

Table 6 Loading patterns and results of specimens

Material	F_{min} (kN)	F_{max} (kN)	S (MPa)	R	log(C)	n	log(C_0)	m_0	γ
Q235B	0.34	33.64	16.65	0.01	-1.990	1.427	-11.155	2.976	0.838
Q235B	7.06	40.36	16.65	0.175	-2.625	1.241			
Q235B	11.1	44.4	16.65	0.25	-1.864	1.585			
Q235B	16.03	49.33	16.65	0.325	0.142	2.421			
Q355B	3.7	37	16.65	0.1	-3.128	1.135	-10.789	2.596	0.715
Q355B	11.1	44.4	16.65	0.25	-2.922	1.270			
Q355B	16.03	49.33	16.65	0.325	-2.065	1.643			

Moreover, the uniform parameters of log(C_1), m_1 and γ for specimens with each material were obtained using the same method and the results were also listed in Table 3 and the fitting effect is shown in Figure 9(c)(d). The figure reveals that the proper parameters of log(C_1), m_1 and γ for each material can lead to rather good fitting effect, since most test results marked in red dot fall into or near the plane with these three parameters. Therefore, the da/dN-ΔS-R equation proposed in this section is well applied to the correlation of fatigue crack growth rate with the SEDF range with the consideration of the stress ratio.

It is worth noting that the mode I fatigue crack growth is the most common crack growth mode in practical engineering structures. Even for many mixed-mode crack problems, the crack growth path often tends to gradually reorient toward a locally opening-dominated mode due to crack deflection mechanisms. Therefore, the proposed da/dN-

Δ*S*-*R* equation was only limited to mode I cracks and the fatigue crack growth tests of CT specimens made of two steels, which represents the most representative and practically significant engineering condition. Nevertheless, further theoretical and experimental investigations on mode II, mode III and mixed-mode crack growth of engineering components made of other materials are still necessary for a more comprehensive validation of the proposed d*a*/d*N*-Δ*S*-*R* equation with the ESEDF approach.

6 CONCLUSION

(1) The proposed ESEDF approach achieves better accuracy than the conventional SEDF approach in regular mode I and mode II crack problems in both 2D and 3D models, as long as sufficiently refined mesh quality at the crack tip (front) is guaranteed, and the results agree well with theoretical solutions as well. However, relatively larger deviations are found in complex 3D mode III crack problems, mixed-mode crack problems and surface crack problems.

(2) The reduced accuracy observed in complex 3D crack problems is primarily due to the serious sensitivity of ESEDF approach to crack-tip mesh quality, crack-front discretization, local field fluctuations and strong singularity, for the ESEDF approach is classified as a local-fracture-parameter-extraction approach. In contrast, the SEDF approach based on interaction integral or J-integral benefits from real and auxiliary field interaction or domain averaging. Therefore, the proposed ESEDF approach directly relies on highly localized crack-tip energy quantities and is more susceptible to numerical errors in complex 3D crack-front conditions.

(3) The ESEDF approach is most suitable to mode I crack problems, mode II crack problems, 2D crack problems, 3D crack problems with simple crack front configurations along with sufficiently refined crack-front mesh, and situations without explicit plane stress/strain assumptions. However, it is less accurate in 3D mode III crack problems, complex 3D mixed-mode crack problems and engineering models with coarse meshing than the conventional SEDF approach, though it is still with acceptable accuracy.

(4) It is recommended to use quadratic singular elements at the crack tip to create a row of sector (prism for 3D) elements with an angle of 10°, a radius of 0.001mm and a prism height within element aspect ratio requirement during the FE analysis to get accurate results for the ESEDF approach, while the mesh sizes are allowed to be sparser to an angle of 15° and a radius of 1mm if very refined meshes cannot be guaranteed. Moreover, a sector radius of 0.333mm can be allowed in 3D FE models in real large-scale engineering structures.

(5) The fatigue test of CT specimens shows good correlations between the fatigue crack growth rate, SEDF range and the stress ratio so that it indicates that the proposed d*a*/d*N*-Δ*S*-*R* equation is well applied to the correlation of fatigue crack growth rate with the SEDF range with the consideration of the stress ratio in mode I fatigue crack growth.

7 LIMITATION AND FUTURE WORK

Although the proposed ESEDF approach demonstrates satisfactory performance for regular mode I and mode II crack problems, some main limitations should still be noted.

(1) The numerical results indicates that the proposed ESEDF approach based on local extraction shows reduced accuracy in complex 3D crack configurations, particularly for mode III, mixed-mode and surface crack problems. This reduction in accuracy is primarily associated with the sensitivity of localized fracture parameter extraction methods to crack-tip mesh quality, crack-front discretization, and local field fluctuations. This limitation will be addressed more in the future work.

(2) The proposed d*a*/d*N*-Δ*S*-*R* equation and its experimental research is limited to mode I fatigue crack growth tests for two steel materials. Therefore, the applicability of the it to mode II, mode III, and mixed-mode fatigue crack growth tests made of other materials still requires further investigation.

(3) In addition to displacement extrapolation, interaction integral and J-integral, XFEM has also become a powerful tool in computing SIF in FE analysis within recent decades. In the future work, XFEM should also be considered in computation of SIF and SEDF in terms of benchmarking.

Nomenclature

Symbol Description

%RA Percentage reduction in area for empirical equation by Badaliance (1980)

a Crack length
A, B, C_1, C_2, C_3, C_4, n Material-dependent constants by Badaliance (1980)
a_{11}, a_{12}, a_{22}, a_{33} Coefficient for calculating SEDF from stress intensity factor (SIF)
a_p Prefabricated crack length in CT specimens
B Thickness of CT specimens
C, n Material-dependent constants for da/dN-ΔS equation
C_0, γ, m_0 Material-dependent constants for da/dN-ΔS-R equation
c_a The distance from the notch tip to the axis of the tensile load in CT specimens
C_p, m_p Constants for Paris law
D_e Mesh density of the mesh-refinement area in FE models
ds Length increment along the contour Γ in J-integral
E Elastic modulus
ER_{ESEDF}, Error of ESEDF approach
$ER_{SEDF\text{-}DE}$ Error of SEDF approach based on displacement extrapolation
$ER_{SEDF\text{-}II}$ Error of SEDF approach based on interaction integral
$ER_{SEDF\text{-}JI}$ Error of SEDF approach based on J-integral
F_{max} Maximum force of the cyclic loading
G Shear modulus
J J-integral for a crack
k Quotient of the numerical SEDF result to the theoretical SEDF result
K_I, K_{II}, K_{III} Stress intensity factor (SIF) for mode I, mode II and mode III cracks
$\overline{K_I}$, $\overline{K_{II}}$, $\overline{K_{III}}$ Mean stress intensity factor (SIF) for mode I, mode II and mode III cracks
K_{max}, K_{min} Maximum and minimum stress intensity factor (SIF)
N Cycle number of cyclic loadings
N_e Element number in the mesh-refinement area
N_{et} Total element number in the model
N_n Node number in the mesh-refinement area
N_{nt} Total node number in the model
r Distance of the location away from the crack tip
R Stress ratio of cyclic loadings
R_d Radius of the mesh-refinement area
R_e Sector radius of sector elements in the first row
S Strain energy density factor (SEDF)
S_{max}, S_{min} Maximum and minimum strain energy density factor (SEDF)
t Sector element thickness
T_i Traction vector components in J-integral
u Nodal displacement along x axis in displacement extrapolation
u_i Displacement vector components in J-integral and interaction integral
u_{ij}^{aux} Auxiliary displacement vector in interaction integral
v Nodal displacement along y axis in displacement extrapolation
V Sector element volume
W Width of the CT specimen (1.25W)
W_t Total strain energy within a sector element
α Empirical parameter in empirical equation by Badaliance (1980)
β Inclination angle of the oblique crack
Γ Integration path around the crack tip in J-integral
ΔK Stress intensity factor (SIF) range
ΔK_I, ΔK_{II}, ΔK_{III} Stress intensity factor (SIF) range for mode I, mode II and mode III cracks
ΔS Strain energy density factor (SEDF) range
Δt Prism element height
ΔW_t Total strain energy within a sector with a volume of ΔV
Δϑ Sector angle of sector elements in the first row
ϑ Polar coordinate for a crack tip
ϑ_0 Crack growth angle in an oblique crack

κ Coefficient for calculation of shear modulus
σ Pressure stress exerted
σ_{ij} Real stress vector at the crack tip in interaction integral
σ_{ij}^{aux} Auxiliary stress vector at the crack tip in interaction integral
σ_u Ultimate strength
σ_y Yield strength
τ Shear stress exerted
υ Poisson's ratio
ω Strain energy density (SED)
$\bar{\omega}$ Average strain energy density (SED) within one sector element

Acknowledgements

This research was sponsored by the National Natural Science Foundation of China (Grant No.52008202), Qing Lan Project and the Cultivation Project of the Jiangsu University Key Laboratory of Intelligent Construction and Smart Operation & Maintenance of Power Infrastructure (Nanjing Institute of Technology).

Author's Contribuitions: Conceptualization, Zhao Fang, Fan Yang and Sheng Shen; Methodology, Zhao Fang, Sheng Shen and Aiqun Li; Investigation, Zhao Fang, Fan Yang, Sheng Shen and Jingwen Yu; Writing - original draft, Zhao Fang; Writing - review & editing; Funding acquisition, Zhao Fang; Resources, Zhao Fang, Fan Yang and Sheng Shen

Data Availability: Research data is only available upon request

Editor: Marco L. Bittencourt

References

Aliha, M. R. M. (2019). On predicting mode II fracture toughness (KIIc) of hot mix asphalt mixtures using the strain energy density criterion. Theoretical and Applied Fracture Mechanics, 99, 36-43.

ASTM E647 (1995), Standard test method for measurement of fatigue crack growth rates. West Conshohocken, PA: American Society for Testing and Materials International.

Ayatollahi, M. R., Moghaddam, M. R., & Berto, F., (2015). A generalized strain energy density criterion for mixed mode fracture analysis in brittle and quasi-brittle materials. Theoretical and Applied Fracture Mechanics, 79: 70-76.

Ayatollahi, M. R., Sedighiani, K., (2012). Mode I fracture initiation in limestone by strain energy density criterion. Theoretical & Applied Fracture Mechanics, 57(1):14-18.

Ayatollahi, M. R., Shadlou, S., & Shokrieh, M. M. (2011). Mixed mode brittle fracture in epoxy/multi-walled carbon nanotube nanocomposites. Engineering Fracture Mechanics, 78(14), 2620-2632.

Badaliance, R., (1980). Application of strain energy density factor to fatigue crack growth analysis. Engineering Fracture Mechanics, 13(3): 657-666.

Berto, F., & Lazzarin, P., (2014). Recent developments in brittle and quasi-brittle failure assessment of engineering materials by means of local approaches. Materials Science and Engineering: R: Reports, 75: 1-48.

Berto, F., Campagnolo, A., Chebat, F., Cincera, M., & Santini, M., (2016). Fatigue strength of steel rollers with failure occurring at the weld root based on the local strain energy values: modelling and fatigue assessment. International Journal of Fatigue, 82, 643-657.

Boulenouar, A., Benseddiq, N., & Mazari, M., (2013). Strain energy density prediction of crack propagation for 2D linear elastic materials. Theoretical and Applied Fracture Mechanics, 67:29-37.

Cao, J., Li, F., Wang, Q., Li, P., & Chen, H. (2016). Analysis of fracture criteria for 7050 aluminum alloy with different geometries based on the elastic strain energy density. Theoretical and Applied Fracture Mechanics, 81, 50-66.

DNVGL-RP-C203 (2016), Fatigue design of offshore steel structures. DET NORSKE VERITAS GL AS.

Erdogan, F., & Sih, G. C. (1963). On the crack extension in plates under plane loading and transverse shear. Journal of Basic Engineering, 85(4):519.

Fajdiga, G., Ren, Z., & Kramar, J. (2007). Comparison of virtual crack extension and strain energy density methods applied to contact surface crack growth. Engineering Fracture Mechanics, 74(17), 2721-2734.

Fang, X. Q., Hu, C., & Huang, W. H. (2007). Strain energy density of a circular cavity buried in a semi-infinite slab of functionally graded materials subjected to anti-plane shear waves. International Journal of Solids and Structures, 44(21), 6987-6998.

Feng, W. J., Liu, Q. F., & Su, R. K. L. (2014). Fracture behaviors of a functionally graded thin superconducting film with transport currents based on the strain energy density theory. Theoretical and Applied Fracture Mechanics, 74, 73-78.

GB/T 6398-2017 (2017), Metallic materials-Fatigue testing-Fatigue crack growth method. Beijing: China Standard Press. (In Chinese)

Hamdi, A., Hocine, N. A., Abdelaziz, M. N., & Benseddiq, N. (2007). Fracture of elastomers under static mixed mode: the strain-energy-density factor. International journal of fracture, 144(2), 65-75.

IIW-2259-15 (2016), Recommendations for fatigue design of welded joints and components. Cham: Springer International Publishing.

Khaji, Z., Fakoor, M., Farid, H. M., & Alderliesten, R. (2022). Applying the new experimental midpoint concept on strain energy density for fracture assessment of composite materials. Theoretical and Applied Fracture Mechanics, 121, 103522.

Lawn, B. R., & Wilshaw, T. R. (1993). Fracture of brittle solids (Vol. 2). London: Cambridge university press.

Lazzarin, P., & Zambardi, R., (2001). A finite-volume-energy based approach to predict the static and fatigue behavior of components with sharp V-shaped notches. International journal of fracture, 112: 275-298.

Li, Y., Fantuzzi, N., & Tornabene, F. (2013). On mixed mode crack initiation and direction in shafts: strain energy density factor and maximum tangential stress criteria. Engineering Fracture Mechanics, 109, 273-289.

Newman Jr, J. C., & Raju, I. S. (1981). An empirical stress-intensity factor equation for the surface crack. Engineering fracture mechanics, 15(1-2), 185-192.

Razavi, N., Aliha, M. R. M., & Berto, F., (2018). Application of an average strain energy density criterion to obtain the mixed mode fracture load of granite rock tested with the cracked asymmetric four-point bend specimens. Theoretical and Applied Fracture Mechanics, 97, 419-425.

Shlyannikov, V., Boychenko, N., Fernandez-Canteli, A., & Muñiz-Calvente, M., (2015). Elastic and plastic parts of strain energy density in critical distance determination. Engineering Fracture Mechanics, 147: 100-118.

Sih, G. C., (1974). Strain-energy-density factor applied to mixed mode crack problems. International Journal of fracture, 10(3): 305-321.

Sih, G. C., Macdonald, B., (1974). Fracture mechanics applied to engineering problems-strain energy density fracture criterion. Engineering Fracture Mechanics, 6(2):361-386.

Sih, G.C., (1984). Fracture mechanics of engineering structural components. In: Sih, G.C., de Oliveira Faria, L. (eds) Fracture Mechanics Methodology. Engineering Applications of Fracture Mechanics, vol 1. Springer, Dordrecht.

Walker, K., (1970). The effect of stress ratio during crack propagation and fatigue for 2024-T3 and 7075-T6 aluminum. ASTM STP,462, 1–14.

Wei, Y., (2012). An extended strain energy density failure criterion by differentiating volumetric and distortional deformation. International Journal of Solids and Structures, 49(9):1117-1126.

Zhou X. P., (2006). Triaxial compressive behavior of rock with mesoscopic heterogenous behavior: SED factor approach. Theoretical & Applied Fracture Mechanics, 45(1):46-63.